Available online at www.sciencedirect.com
ScienceDirect
Journal of the European Ceramic Society 29 (2009) 31–38
www.elsevier.com/locate/jeurceramsoc

Contribution to porous mullite synthesis from clays by adding Al and Mg powders

A. Esharghawi, C. Penot, F. Nardou *

SPCTS, CNRS, UMR 6638, Université de Limoges, 123 Avenue Albert Thomas, 87060 Limoges Cedex, France

Received 15 October 2006; received in revised form 25 April 2008; accepted 2 May 2008
Available online 14 July 2008

Abstract

This work has been undertaken to consider the production of porous mullite from kaolinitic clays. X-ray diffraction, scanning electron microscopy, thermogravimetry, differential thermal and dilatometry analyses were performed to study their thermal behavior. Pure and porous mullite was obtained by adding aluminum metal powder to kaolinite and hot processing in oxidizing atmosphere. Comparative studies were carried out to evaluate the influence of various weight ratios of magnesium on both the formation and reactive sintering of mullite. Porosity was shown to be increased with magnesium content while needle-like mullite crystals could be observed.

Keywords: Sintering; Porosity; Clays; Mullite; Al; Mg

1. Introduction

Porous refractory materials with high temperature applications are of great interest today (insulators, catalyst supports, filters, etc.). They can be produced by various techniques, generally by addition of organic pore-forming agents[1] but also starting from foams[2] or by sol–gel synthesis.[3] Ebadzadeh[4] used aluminum to produce a mullite–zirconia composite by reactive sintering of zircon and aluminum powder, and observed that porosity was due to aluminum oxidation.

It is well known that mullite ($3Al_2O_3{\cdot}2SiO_2$) is the only stable compound in the system SiO_2–Al_2O_3.[5,6] Due to its good physical properties[7–10] (low thermal expansion coefficient, good thermal stability, creep resistance, etc.) it is a very attractive compound for dense or porous material applications but the different methods of synthesis are often expensive. Clays and in particular kaolinite ($Al_2O_3{\cdot}2SiO_2{\cdot}2H_2O$), are very advantageous minerals for mullite synthesis due to their low cost. Because of the higher content of silica in clays than in mullite, it is necessary to add aluminum oxide in order to obtain the stoichiometric mullite composition. This enrichment is generally made by alumina[8,9,11,12] or aluminum hydroxide[13,14] additions. Mullite production from these powder mixtures requires high temperature treatments[11] (1500–1600 °C) for several hours. Other authors[15,16] used aluminum metal powder/clay mixtures and applied the same heat treatment.

In order to obtain pure porous mullite bodies we chose to start from a mixture of only aluminum/clay. Moreover, because MgO enhances both the formation and sintering of mullite[10,17–19] we will introduce various ratios of magnesium metal powder in order to study both the effect of magnesium oxidation on porosity created by Al oxidation and reactive sintering of mullite.

2. Experimental procedure

We used raw Saharan clay whose average chemical composition was given in Table 1. The powders dried for 24 h at 110 °C then were ball-milled in air with alumina balls in order to obtain a homogeneous powder without agglomeration. The grain size of the clay was very little modified by ball-milling and, finally, pretreated clay was obtained.

Three batches named A, B, and C (Table 2) and containing the pretreated clay and Al–Mg, were prepared by mixing 89.5 wt% of clay with 10.5 wt% of aluminum powder (purity 99%, average grain size <45 μm, provided by CERAC) and various small amounts of magnesium powder (purity 98%, average grain size 250 μm, provided by VWR International) in order to

* Corresponding author. Tel.: +33 555457487; fax: +33 555457586.
E-mail address: francoise.nardou@unilim.fr (F. Nardou).

0955-2219/$ – see front matter © 2008 Elsevier Ltd. All rights reserved.
doi:10.1016/j.jeurceramsoc.2008.05.036

Table 1
Chemical composition of clay (wt%)

Loss on ignition	12.23
SiO_2	51.32
Al_2O_3	30.77
Fe_2O_3	1.93
TiO_2	1.76
CaO	0.06
MgO	0.03
K_2O	0.10

Table 2
Composition of the different batches (wt%)

Mixture	A	B	C
Clay	89.5	89.5	89.5
Aluminum	10.5	10.5	10.5
Magnesium	0	1	3

obtain respectively 0, 1, or 3 wt% of Mg. Each batch was ground for 13 h in ethanol using a FRITSCH planetary ball-mill (pulverisette 6) at 280 rpm and the slurry obtained was then dried at 100 °C for 24 h.

Cylindrical pellets of each batch (A, B, and C) were processed using uniaxial pressing at about 200 MPa (average green density: 1.50). These compacts were sintered in air using a NABERTHERM LHT 04/17 furnace. The firing was carried out with a heating rate of 5 °C/min up to 1100 °C and then of 10 °C/min above 1100 °C to the dwell temperature (1400–1550 °C). The latter was maintained for 5 h before cooling to room temperature (10 °C/min).

The thermal behavior of raw clay and different batches was tested by differential thermal (DTA) and thermogravimetry (TG) analyses on SETARAM devices. We used a LINSEIS dilatometer type L75 to determine the thermal expansion of square section bar (0.5 cm × 0.5 cm × 2 cm) samples shaped by uniaxial pressing (100 MPa). All the thermal analyses (dilatometry, TG and DTA) were carried out in air at a heating rate of 10 °C/min. After vacuum degasification at 200 °C for several hours, the BET specific surface area of powders was evaluated in nitrogen using a MICROMERITICS ASAP 2000 device. The identification of the crystalline phases was carried out by X-ray diffraction (XRD) with a Cu Kα radiation (SIEMENS D 5000). The morphology of both powders and sintered bodies, polished and thermally etched, was investigated by scanning electron

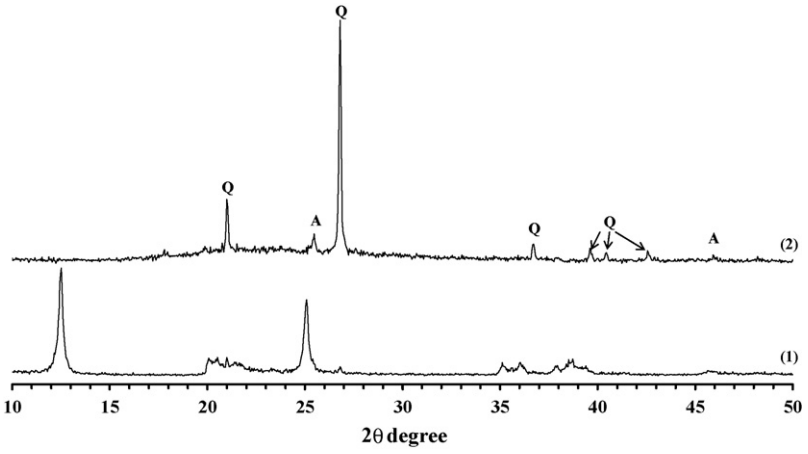

Fig. 1. XRD pattern of the mixture of clays: (1) before heat treatment and (2) heat treated at 650 °C (A = anatase, Q = quartz).

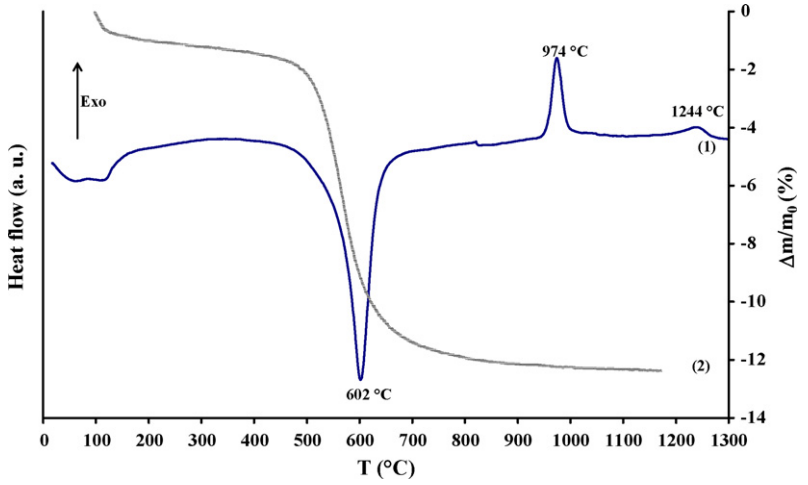

Fig. 2. Thermal behavior of pure clay: (1) ATD and (2) TG curves.

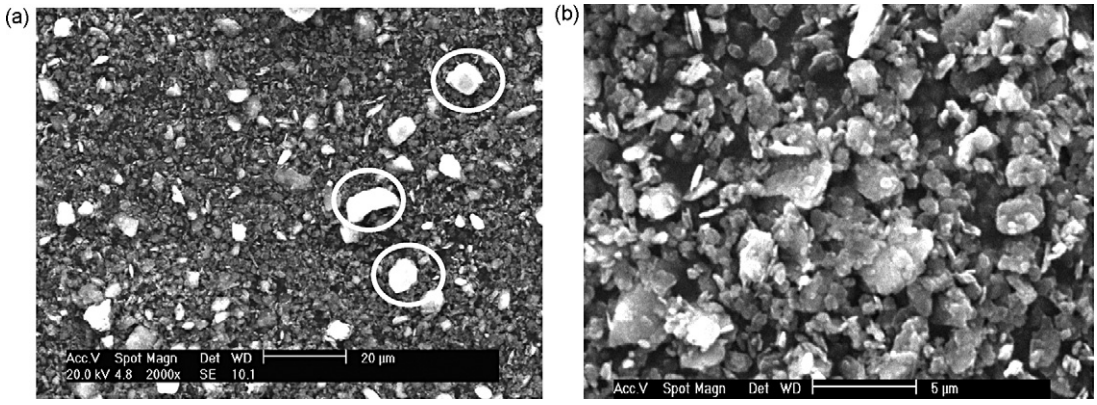

Fig. 3. SEM micrographs of raw clay powder mixture showing: (a) bright quartz particles and (b) clays agglomerates.

microscopy (SEM) with PHILLIPS XL30 equipment working at 20 kV. Bulk densities of the sintered pellets were evaluated by geometrical measurements.

3. Results and discussion

3.1. Characterization of raw clay and aluminum powder

3.1.1. Raw clay

XRD analysis of the clay before applying heat treatment showed that kaolinite was the major mineral component with a small amount of free quartz impurities (Fig. 1). After calcination of the clay at 650 °C the only crystalline phases visible were α-SiO_2 and TiO_2-anatase which was often associated with kaolinite.[20] Thermal behavior, illustrated in Fig. 2, was characterized by typical DTA and TG curves of kaolinite with: (i) two endothermic effects located at about 120 °C and 602 °C and associated with corresponding weight losses; (ii) two exothermic effects occurring at 974 °C and 1244 °C, not associated with any change of weight.

The last ATD peaks can be assigned respectively to:

- reorganization of metakaolin into a spinel-type phase,[21]
- crystallization of mullite.

The two first ATD peaks correspond respectively to:

- dehydration of the clay at about 120 °C,
- dehydroxylation at 602 °C.

The global loss of weight characteristic of these last two reactions is about 12%.

SEM observations of Fig. 3a at low magnification showed quartz crystals which appeared as bright and large particles with a size below 20 μm. They are dispersed among agglomerates of lamellar particles of clay. The size of these agglomerates ranges from 1 to 5 μm.

The value of the specific surface area was of 15 m^2/g after a dynamic vacuum heat treatment (150 °C) for 4 h. This BET value could be associated to a crystallite size of about 0.15 μm if the particles are supposed spherical.

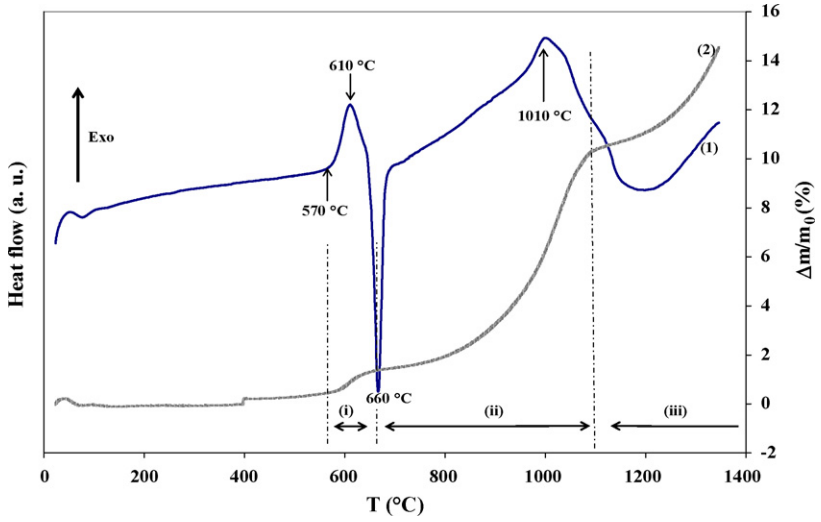

Fig. 4. Thermal behavior of pure aluminum powder: (1) DTA and (2) TG curves.

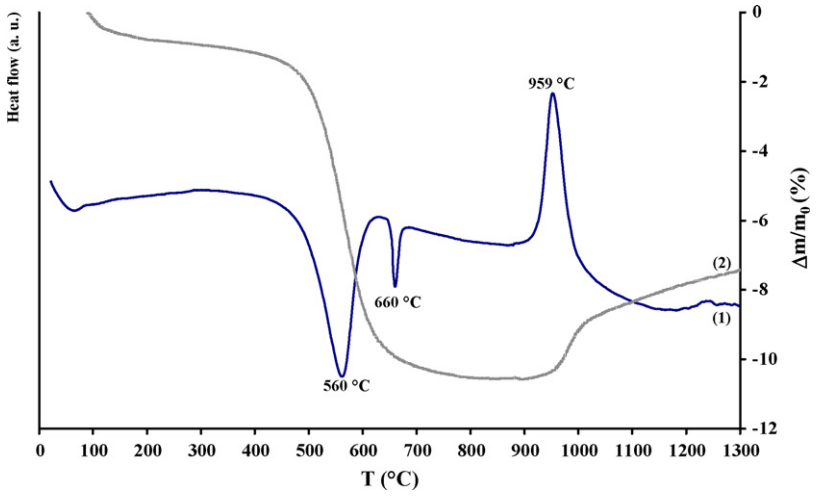

Fig. 5. Thermal behavior of the clay/Al mixture: (1) DTA and (2) TG curves.

3.1.2. Aluminum powder

The DTA and TG curves of aluminum powder (Fig. 4) highlighted three areas: (i) the solid-state oxidation of aluminum at ≈600 °C up to the Al melting at 660 °C, (ii) the liquid-state aluminum oxidation from 660 to about 1030 °C, as it was previously observed by other authors,[4,11] (iii) a liquid-state post-oxidation of Al over 1200 °C. All these phenomena were associated with a weight gain from 570 to 1400 °C and accelerations of weight gain were visible in each domain.

Trunov et al.[22,23] explains these various stages of aluminum oxidation by the polymorphic phase transformations that occurred inside the film of aluminum oxide: Al powders were naturally coated by a layer of amorphous alumina which was more stable than crystalline alumina phases as long as its thickness did not exceed a critical value. During heating, amorphous alumina crystallized successively into γ-Al_2O_3 and then into α-Al_2O_3 about 1000 °C. But this last transformation between γ and α might be carried out via δ-Al_2O_3 and then θ-Al_2O_3. These transformations can be broadly summarized as follows:

$$\text{Amorphous}\quad Al_2O_3 \rightarrow \gamma\text{-}Al_2O_3 \rightarrow (\delta\text{-}Al_2O_3 \rightarrow \theta\text{-}Al_2O_3 \rightarrow) \alpha\text{-}Al_2O_3$$

In our study we did not observe the δ and θ phases when aluminum powders were heat treated.

So in solid phase oxidation can be regarded as enhanced via microcracks[4] of the amorphous alumina layer. These cracks were generated by the difference between the thermal expansion coefficients of solid aluminum ($\alpha = 25 \times 10^{-6}\,K^{-1}$) and amorphous alumina ($\alpha = 8.3 \times 10^{-6}\,K^{-1}$).

After the aluminum melting (660 °C), the volume dilatation of Al liquid is much larger ($\Delta V = +6.26\%$)[24] than that of Al metal and this initiates more cracks in the alumina layer which accelerates the oxidation as it can be observed. At the same time crystallization of amorphous alumina into γ-Al_2O_3 could develop. As the specific volume of γ-Al_2O_3 is smaller than that of amorphous alumina the cracking of the oxide layer would be enhanced, which increased the oxidation rate up to 1000 °C.

Beyond this temperature the oxidation rate slowed down when the phase transformation γ → α occurred because α-alumina was more compact than γ-alumina[22] so the alumina layer was more efficient as a barrier of diffusion and the oxidation rate decreased. When the heating up was carried out the diffusion was activated and the oxidation of aluminum increased again.

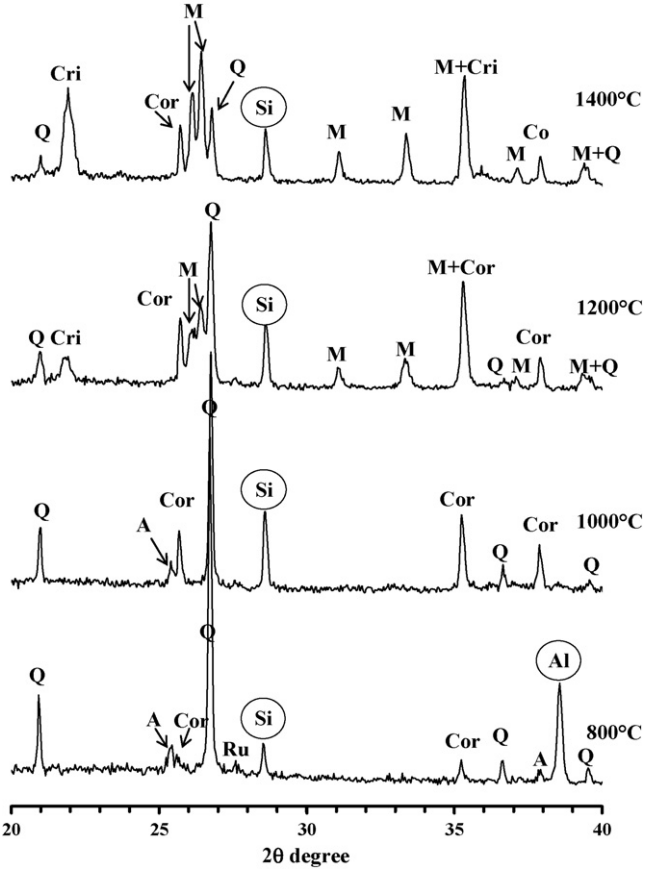

Fig. 6. XRD patterns of sample of clay/10.5 wt% aluminum heat treated at different temperatures and rapidly quenched to room temperature (Q = quartz, Al = aluminum, A = anatase, Ru = rutile, Si = silicon, Cor = corindon, Cri = cristobalite, M = mullite).

Table 3
Crystallographic evolution of the mixture clay/aluminum powder

Phases	Pure clay (700 °C)	800 °C	900 °C	1000 °C	1100 °C	1200 °C	1300 °C	1400 °C
Quartz	+++	+++	+++	+++	++	++	+	
Cristobalite							+	+
Si		+	+	++	++	++	+	+
Al		++	+	?				
α-Al_2O_3		+	+	++	++	++	+	+
Anatase	+	+	+	+				
Rutile		+	+	+	+	++		
Mullite						+	++	+++

3.2. Elaboration of porous mullite from clay/Al mixture

The addition of aluminum powder to the clay strongly modified its thermal behavior as it could be seen on the DTA–TG curves of the mixture (clay/10.5 wt% Al) heated in air (Fig. 5). Aluminum oxidation which started near 600 °C for pure Al now boosted the dehydroxylation of the clay as the position of the correspondent peak was moving from 602 to 560 °C and the associated weight loss was reduced to about 10 wt%. Melting of aluminum was always visible at 660 °C while metakaolin transformation occurred now about 959 °C instead of 974 °C. This exothermic effect was associated to a significant weight gain which could be attributed to an increase of aluminum oxidation rate (previously noted in Fig. 4).

In order to follow the crystalline evolution of phase, samples were heat treated at different temperatures (800–1400 °C) and rapidly quenched in air to room temperature. The DRX analysis (Fig. 6 and Table 3) showed: (i) a precipitation of Si produced by reduction of SiO_2 contained in the clay by aluminum, a later gas/solid oxidation of Si leading to mullite formation; (ii) the Al oxidation which started above 570 °C as previously noted continued to 1000 °C with formation of α-alumina; (iii) quartz is present up to 1400 °C but gradually disappeared with the formation of cristoballite starting at 1300 °C; (iv) α-alumina increased gradually to 1200 °C, at this temperature mullite formation occurred and thus α-Al_2O_3 disappeared progressively; (v) anatase initially present in clay, at 1100 °C transformed into rutile phase which disappeared with mullite formation. On the contrary, samples obtained by reactive sintering for 5 h at 1550 °C showed (Fig. 7) that mullite was the only crystalline phase in agreement with JCPDS 15-0776.

Dilatometric analyses (Fig. 8) show that sintering starts near 1200 °C. For the bar-shaped sample containing clay with 10.5 wt% of Al, the relative shrinkage was smaller than that observed with raw clay, the values reaching respectively 11 and 19.6% for heating up to 1350 °C.

Table 4
Densities of the different sintered bodies

Sintering temperature	Density		Porosity (%)
	1400 °C	1550 °C	1550 °C
Mixture A	2.18	2.23	30
Mixture B	2.19	2.03	36
Mixture C	2.10	1.35	58

The densities of sintered bodies obtained from clay/Al mixture as pellets fired at 1400 and 1550 °C for 5 h (Table 4), are in agreement with the dilatometric curves. The relative densities are not very high and reached a maximum of 70% of mullite theoretical density (3.17) for the samples sintered at 1550 °C. Otherwise when the pellets are sintered at 1400 °C they are constituted, in addition of mullite, of small amounts of corundum ($d = 3.99$) and of cristobalite ($d = 2.33$) so one cannot compare their density with that of mullite.

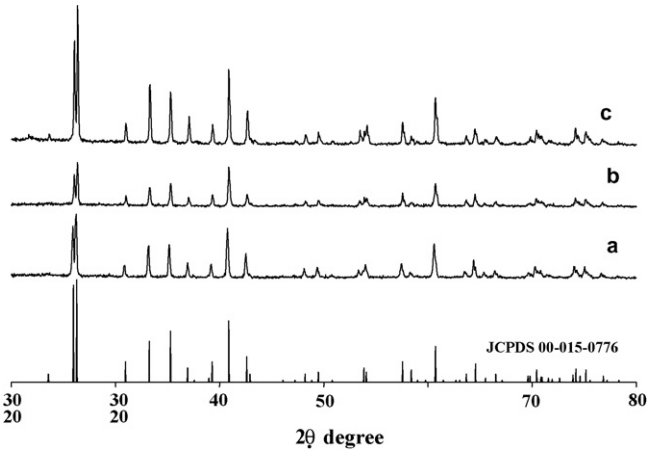

Fig. 7. XRD patterns of the different samples of clay with 10.5 wt% aluminum and various amounts of magnesium powder sintered at 1550 °C for 5 h with (a) 0% Mg, (b) 1% Mg and (c) 3% Mg. Only mullite diffraction peaks are clearly visible.

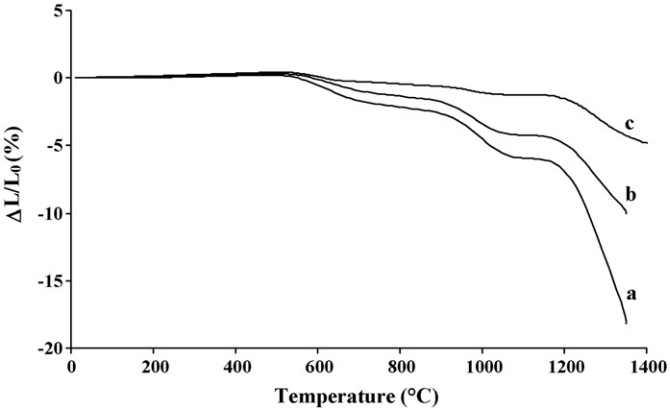

Fig. 8. Dilatometric analysis of: (a) pure raw clay; (b) raw clay +10.5 wt% Al; (c) raw clay +10.5 wt% Al + 3 wt% Mg.

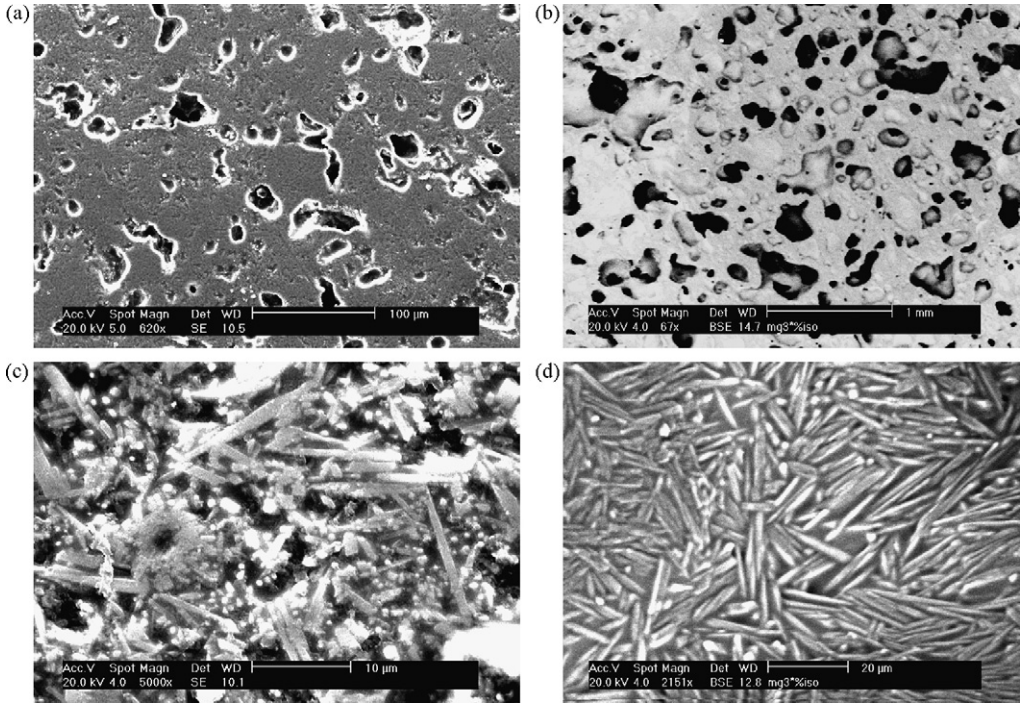

Fig. 9. SEM micrographs of uniaxial pressed compacts sintered at 1550 °C for 5 h showing: (a) and (c) a sample with 0% Mg; (b) and (d) a sample with 3% Mg.

Porosity is considerable and SEM observations (Fig. 9a) show spherical cavities sized about 30 μm. One can suppose that these small voids are created at the initial aluminum grain sites during Al oxidation. Due to the large particle size of the aluminum powder (smaller than 45 μm) the major part of the aluminum oxidation occurred in the liquid phase domain. To be complete in the solid phase domain, the oxidation of Al powders should require a particle size lower than 1 μm[4,25] but with fine grains the combustion should be very fast as an auto-combustion reaction.[26]

3.3. Effect of magnesium addition

The addition of magnesium drastically modified the thermal phenomena that normally occur during heating of a mixture clay/Al (Fig. 10). One can note (Fig. 10B and C) that magnesium oxidation is characterized by an exothermic effect occurring near 629 °C and all the more marked since the Mg content is higher. The peak related to the crystallization of mullite and approximately localized at 1240 °C for pure clay has completely disappeared which was undoubtedly due to its very low amplitude. Otherwise, it can be noted that Mg, like Al, could interact with silica to give magnesia and silicon.

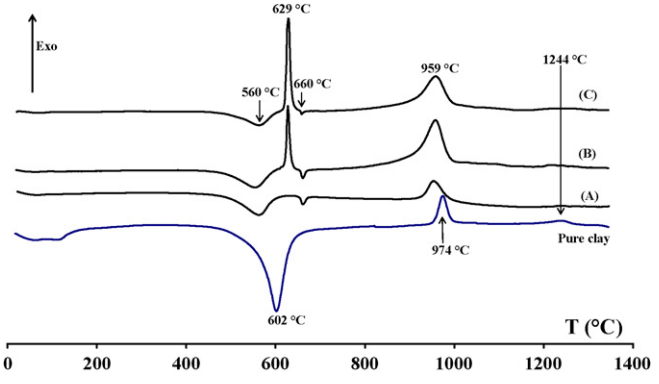

Fig. 10. DTA curves taken in air of raw clay/aluminum powder mixtures containing various wt% of magnesium powder: (A) 0%; (B) 1%; (C) 3%.

If we consider the enthalpy of formation of each oxide, respectively $\Delta H^{\circ}_{Al/Al_2O_3} = -1675.7\,kJ\,mol^{-1}$ and $\Delta H^{\circ}_{Mg/MgO} = -601.6\,kJ\,mol^{-1}$,[27] it is surprising to have a more marked thermal effect for the oxidation of Mg than for the Al one. It can be explained by their values of the coefficient of Pilling and Bedworth, respectively $\Delta_{Al_2O_{3\alpha}} = 1.286$ and $\Delta_{MgO} = 0.806$. So, because of its $\Delta > 1$ alumina may play the role of a diffusion barrier for oxygen during the oxidation of Al and could reduce the rate of oxidation. On the contrary magnesia, with a $\Delta < 1$, cannot monitor the oxidation of magnesium. The oxidation of Al is very slow after the formation of the thin layer of amorphous Al_2O_3 and the rate of reaction is monitored by the volume diffusion through the alumina layer. On the contrary, the oxidation reaction of Mg is very quick and the rate of the reaction is only controlled by the reaction at the interface metal/gas.

Dilatometric curves (Fig. 8c) were the same for mixtures containing 1% (not presented here) or 3% of magnesium. As for clay/Al mixture, the shrinkage began at 1200 °C. At 1350 °C the shrinkage was reduced to 7.7% for each of the samples containing Mg instead of 11% without Mg. After sintering 5 h at 1550 °C the thermal expansion coefficient of a bar shaped sample measured in the range 20–1000 °C was of $5.3 \times 10^{-6}\,K^{-1}$ which is slightly higher than what is expected for dense mullite ($4 \times 10^{-6}\,K^{-1}$).

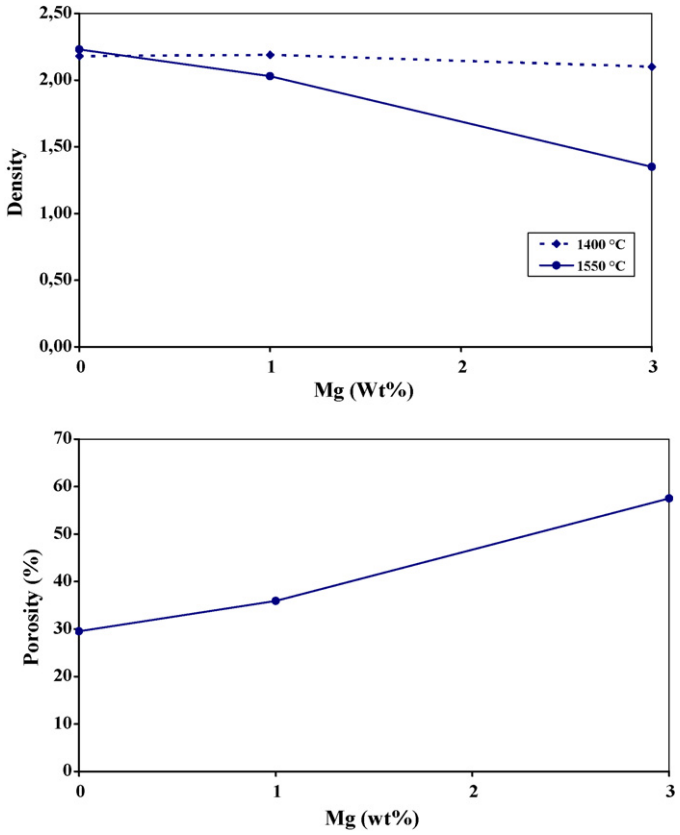

Fig. 11. Density evolution of sintered bodies with magnesium content. Porosity evolution of samples sintered 5 h at 1550 °C with magnesium content.

By adding 3 wt% Mg the values of densities of the sintered bodies (Table 4), were respectively of 66 and 42% of mullite theoretical density at 1400 and 1550 °C. The density decreased when sintering temperature increased from 1400 to 1550 °C (Fig. 11). Similar results have been obtained by Ebadzadeh[4] for the elaboration of mullite-zirconia composites. If we remind that pure mullite was only obtained after sintering at 1550 °C while at 1400 °C other denser phases as alumina where still present, one could explain this reducing of density from 1400 to 1550 °C.

The percentage of porosity for the samples sintered at 1550 °C for 5 h was calculated using the following equation:

$$\%\,\text{porosity} = \frac{V_P - V_M}{V_P} \times 100$$

where V_P was the volume of the pellet obtained by geometrical measurements and V_M the volume of mullite deduced from the weight of the pellet (m_P) and the theoretical density of mullite ($d_M = 3.17$):

$$V_M = \frac{m_P}{d_M}$$

So, Fig. 11 showed that it increased when magnesium ratio increased.

Indeed, as for clay/Al mixture without magnesium, SEM observations (Fig. 9b) showed now two sizes of porosity: one of 30 μm and another one sized about 320 μm. If the first one could be created by Al oxidation, the second one was probably due to magnesium oxidation because, although higher, it was ranging in the size of Mg particles (230 μm). This would suggest that porosity of sintered bodies could be monitored by adding amounts of Al and Mg metal powders with fixed grain size. Micrographs of higher magnification (Fig. 9c and d) highlighted needle shape crystallites of mullite which appeared after sintering (5 h at 1550 °C). These acicular crystals were all the more marked since the magnesium content was higher. So the addition of small amounts of Mg powder would cause not only another porosity depending on the Mg grain size but also the germination of an acicular mullite phase. Otherwise addition of Mg reduced reactive sintering of mullite and increased porosity (from 30 to 58%) even if magnesium oxidation brought thermal energy (Table 3).

4. Conclusions

The synthesis of pure and porous mullite has been shown to be possible by adding aluminum powder to kaolinitic clay before sintering in air. The exothermic oxidation reaction of aluminum would provide energy for germination of α-alumina phase which then reacts with metakaolin to form the mullite phase. The bodies obtained by reactive sintering at 1550 °C have a high open porosity initiated during the oxidation of aluminum powder. This porosity increases when a small amount of magnesium powder is added. In spite of this high porosity the sintered bodies have a good mechanical cohesion.

References

1. Barea, R., Osendi, M. I., Ferreira, J. M. F. and Miranzo, P., Thermal conductivity of highly porous mullite material. *Acta Mater.*, 2005, **53**, 3313–3318.
2. Juettner, T., Moertel, H., Svinka, V. and Svinka, R., Structure of kaoline-alumina based foam ceramics for high temperature applications. *J. Eur. Ceram. Soc.*, 2007, **27**, 1435–1441.
3. Shuqiang, D., Yu-Ping, Z. and Dongliang, J., Fabrication of mullite ceramics with ultrahigh porosity by gel freeze drying. *J. Am. Ceram. Soc.*, 2007, **90**, 2276–2279.
4. Ebadzadeh, T., Porous mullite–ZrO_2 composites from reaction sintering of zircon and aluminum. *Ceram. Int.*, 2005, **31**, 1091–1095.
5. Pask, J. A., In *Current Understanding of Stable and Metastable Phase Equilibria and Reactions in the SiO_2-αAl_2O_3 System, Ceramics Powders*, ed. P. Vincenzini. Elsevier Scientific Publishing Company, Amsterdam, Oxford, New York, 1983, pp. 21–31.
6. Pask, J. A., Importance of starting materials on reactions and phase equilibria in the Al_2O_3–SiO_2 system. *J. Eur. Ceram. Soc.*, 1996, **16**, 101–108.
7. Schneider, H., Schreuer, J. and Hildmann, B., Structure and properties of mullite—a review. *J. Eur. Ceram. Soc.*, 2008, **28**, 329–344.
8. Viswabaskaran, V., Gnanam, F. D. and Balasubramanian, M., Mullitisation behaviour of calcined clay–alumina mixtures. *Ceram. Int.*, 2003, **29**, 561–571.
9. Goski, D. G. and Caley, W. F., Reaction sintering of kyanite and alumina to form mullite composites. *Can. Metal. Q.*, 1999, **38**, 119–126.
10. Montanaro, L., Tulliani, J. M., Perrot, C. and Negro, A., Sintering of industrial mullites. *J. Eur. Ceram. Soc.*, 1997, **17**, 1715–1723.
11. Viswabaskaran, V., Gnanam, F. D. and Balasubramanian, M., Mullitisation behaviour of south Indian clays. *Ceram. Int.*, 2002, **28**, 557–564.
12. Chen, C. Y., Lan, G. S. and Tuan, W. H., Preparation of mullite by the reaction sintering of kaolinite and alumina. *J. Eur. Ceram. Soc.*, 2000, **20**, 2519–2525.
13. Liu, Y.-F., Liu, X.-Q., Tao, S.-W., Meng, G.-Y. and Sorensen, O. T., Kinetics of the reactive sintering of kaolinite-aluminum hydroxyde extrudate. *Ceram. Int.*, 2002, **28**, 479–486.

14. Pascual, J., Zapatero, j., Jiménez de Haro, M. C., Varona, I., Justo, A., Pérez-Rodríguez, J. L. *et al.*, Porous mullite and mullite-based composites by chemical processing of kaolinite and aluminium metal wastes. *J. Mater. Chem.*, 2000, **10**, 1409–1414.
15. Balmori-Ramírez, H., Rocha-Rangel, E., Refugio-García, E. and Bradt, R. C., Dense mullite from attrition-milled kyanite and aluminum metal. *J. Am. Ceram. Soc.*, 2004, **87**, 144–146.
16. Khabas, T. A., Nevvonen, O. V. and Vereshchagin, V. I., Synthesis of mullitein the presence of nanodisperse aluminum powder. *Refract. Ind. Ceram.*, 2005, **46**, 71–75.
17. Viswabaskaran, V. and Gnanam, F. D., Effect of MgO on mullitisation behavior of clays. *J. Mater. Sci. Lett.*, 2003, **22**, 663–668.
18. Kong, L. B., Chen, Y. Z., Zhang, T. S., Ma, J., Boey, F. and Huang, H., Effect of alkaline-earth oxides on phase formation and morphology development of mullite ceramics. *Ceram. Int.*, 2004, **30**, 1319–1323.
19. Heraiz, M., Merrouche, A. and Saheb, N., Effect of MgO addition and sintering parameters on mullite formation through reaction sintering kaolin and alumina. *Adv. Appl. Ceram.*, 2006, **105**, 285–290.
20. Caillère, S., Hénin, S. and Rautureau, M., *Minéralogie des argiles*. Masson, Paris, 1982, tome 2, 26.
21. Lee, W. E., Souza, G. P., McConville, C. J., Tarvornpanich, T. and Iqbal, Y., Mullite formation in clays and clay-derived vitreous ceramics. *J. Eur. Ceram. Soc.*, 2008, **28**, 465–471.
22. Trunov, M. A., Schoenitz, M., Zhu, X. and Dreizin, E. L., Effect of polymorphic phase transformations in Al_2O_3 film on oxidation kinetics of aluminum powders. *Combust. Flame*, 2005, **40**, 310–318.
23. Trunov, M. A., Umbrajkar, S. M., Schoenitz, M., Mang, J. T. and Dreizin, E. L., Oxidation and melting of aluminum nanopowders. *J. Phys. Chem. B*, 2006, **110**, 13094–13099.
24. Pascal, P., *Nouveau Traité de Chimie Minérale*. Masson, Paris, 1962, tome VI, 490.
25. Holz, D., Wu, S., Scheppokat, S. and Claussen, N., Effect of processing parameters on phase and microstructure evolution in RBAO ceramics. *J. Am. Ceram. Soc.*, 1994, **77**, 2509–2517.
26. Kwon, Y.-S., Gromov, A. A., Ilyin, A. P., Popenko, E. M. and Rim, G.-H., The mechanism of combustion of superfine aluminum powders. *Combust. Flame*, 2003, **133**, 385–391.
27. *Handbook of Chemistry and Physics* (*72nd ed.*). CRC Press, USA, 1991–1992, 5–7 and 5–8.